AIAA-2001-0908
Reynolds Number Effects on the Performance of Ailerons and Spoilers (Invited)

R. E. Mineck
NASA Langley Research Center
Hampton, Virginia

39th AIAA Aerospace Sciences Meeting & Exhibit
8-11 January 2001
Reno, Nevada

For permission to copy or republish, contact the American Institute of Aeronautics and Astronautics
1801 Alexander Bell Drive, Suite 500, Reston, VA 20191-4344

AIAA-2001-0908

REYNOLDS NUMBER EFFECTS ON THE PERFORMANCE OF AILERONS AND SPOILERS

R. Mineck*
NASA Langley Research Center
Hampton, VA

Abstract

The influence of Reynolds number on the performance of outboard spoilers and ailerons was investigated on a generic subsonic transport configuration in the National Transonic Facility over a chord Reynolds number range from 3 to 30 million and a Mach number range from 0.70 to 0.94. Spoiler deflection angles of 0, 10, and 20 degrees and aileron deflection angles of -10, 0, and 10 degrees were tested. Aeroelastic effects were minimized by testing at constant normalized dynamic pressure conditions over intermediate Reynolds number ranges. Results indicated that the increment in rolling moment due to spoiler deflection generally becomes more negative as the Reynolds number increases from 3×10^6 to 22×10^6 with only small changes between Reynolds numbers of 22×10^6 and 30×10^6. The change in the increment in rolling moment coefficient with Reynolds number for the aileron deflected configuration is generally small with a general trend of increasing magnitude with increasing Reynolds number.

Nomenclature

All dimensional data are presented in U.S. customary units. The longitudinal force and moment data are presented in coefficient form in the stability axis system. The lateral moment data are presented in coefficient form in the body axis system. The symbols and abbreviations are defined as follows:

c	local chord
C_L	lift coefficient
C_l	rolling moment coefficient
C_m	pitching-moment coefficient
C_n	yawing moment coefficient
$C_{p,te}$	static pressure coefficient at the wing trailing edge
M_∞	free stream Mach number
q_∞/E	ratio of free stream dynamic pressure to wing material modulus of elasticity
$R_{\bar{c}}$	Reynolds number based on mean geometric chord
sta	model streamwise station, in.
T_t	stagnation temperature, °F
α	angle of attack, deg
Δ	change in a parameter
δ_a	aileron deflection, positive trailing edge down, deg
δ_s	spoiler deflection, deg
η	wing semispan fraction

Background

Lateral control devices are typically designed using empirical tools, analytical methods, and wind tunnel tests. Conventional wind tunnel tests typically provide results at Reynolds numbers significantly below those encountered in flight. Thus, some form of adjustment may be needed to account for the effects of Reynolds number on the results. A series of wind tunnel tests were undertaken to investigate the effect of Reynolds number on the performance of ailerons and spoilers on a generic subsonic transport configuration.

The generic wing-body configuration used in the wind tunnel tests was representative of a subsonic commercial transport configuration. The body was the Pathfinder-I fuselage described in reference 1. The wing, referred to as the Pathfinder-I Lateral Controls Wing, was based on the Energy Efficient Transport (EET) configuration, described in reference 1. The Lateral Controls Wing had provisions for mounting inboard spoilers and ailerons and outboard spoilers and ailerons. Pressure orifices were installed in chordwise rows on the wing and along the wing trailing edge.

This paper presents results from two wind tunnel tests that investigated the effects of Reynolds number on the performance of outboard spoilers and outboard

*Aerospace Engineer; Subsonic Aerodynamics Branch

Copyright (c) 2001 by the American Institute of Aeronautics and Astronautics, Inc. No copyright is asserted in the United States under Title 17, U.S. Code. The U.S. Government has a royalty-free license to exercise all rights under the copyright claimed herein for Governmental purposes. All other rights are reserved by the copyright owner.

ailerons. Results are presented at Mach numbers of 0.70, 0.82, 0.88, and 0.94 at chord based Reynolds numbers of 3×10^6, 13×10^6, 22×10^6, and 30×10^6.

Experimental Apparatus

Test Facility

The National Transonic Facility (NTF) is a fan-driven, closed-circuit, continuous-flow, pressurized wind tunnel (ref. 2). It may be operated as a conventional wind tunnel using air as a test gas or as a cryogenic wind tunnel using nitrogen as a test gas. When operated as a conventional wind tunnel, heat is removed by a water-cooled heat exchanger located at the upstream end of the settling chamber. When operated as a cryogenic tunnel, heat is removed by the evaporation of liquid nitrogen which is sprayed into the tunnel circuit ahead of the fan. Nitrogen gas is vented to maintain a constant total pressure. NTF capabilities allow testing of aircraft configurations at Mach numbers ranging from low subsonic to low supersonic, at Reynolds numbers up to full-scale flight values (depending on aircraft type and size). The test section is 8.2 feet by 8.2 feet in cross section and 25 feet in length. Longitudinal slots in the floor and ceiling give a wall-openness ratio of 6 percent. The test-section sidewalls are solid. The NTF is capable of an absolute pressure range from 15 psi to 125 psi, a stagnation temperature range from −320°F to 150°F, a Mach number range from 0.2 to 1.2, and a maximum Reynolds number per foot of 146×10^6 at Mach 1.

Free stream turbulence is reduced by four damping screens and the 15:1 contraction ratio between the settling chamber and the test section. An initial assessment of the flow quality in the NTF has been reported in reference 3. Conventional model support is provided by an aft-mounted sting attached to a vertically mounted arc sector. The pitch range of the arc sector is from about -11° to 19°, depending on the test setup. A remotely controlled roll coupling, with a range from -180° to 180°, provides the interface between the arc sector and the sting. The test-section floor, ceiling, and reentry flap angles were fixed during these tests.

Model Description

The generic low-wing subsonic transport wing known as the NTF Pathfinder-I Lateral Controls Wing was used in this investigation. The wing is designed for use with the existing NTF Pathfinder-I subsonic transport model fuselage components (ref. 1). A 10.5-inch fuselage extension plug was inserted between the nose and wing to provide a more realistic ratio of fuselage length to wing span. Wing-fuselage fillets typical of current subsonic transport designs were installed at the wing root. The model is designed to accept inboard and outboard spoilers and ailerons. Sketches of the model general arrangement, the outboard spoilers, and the outboard ailerons are presented in figure 1.

The wing design, based on the EET wing reported in reference 1, incorporated supercritical airfoil sections with blunt trailing edges. It was manufactured from Vascomax T-200 steel and had a surface finish of 8 microinches for the first 15-percent of the local chord and 16 microinches for the remainder. The planform break is located at $\eta = 0.376$, with extended chord lengths inboard of this station. (See figure 1(a)). Wing attributes, presented in table 1, were based on the trapezoidal reference planform formed by extending the outboard leading and trailing edge lines to the centerline and to the wing tip station. The cruise design condition is for a lift coefficient of 0.55 at a Mach number of 0.82. Because the wind tunnel model is not a scaled representation of a full scale aircraft, a cruise Reynolds number is not defined. The rear, outboard portion of the port wing panel was removable so that different pieces simulating different outboard aileron deflections could be installed. Provisions were also made to install spoilers on the center portion of the port wing panel.

The outboard spoilers consisted of two panels for the two spoiler deflections: 10° and 20°. Details about the spoilers are presented in figure 1(b). The spoiler panels were removed for the 0° deflection case. When installed, each spoiler panel was sealed to the wing surface to prevent any flow from going between the spoiler panel and the wing upper surface. The two spoiler panels were always installed with the same deflection angle.

The outboard aileron consisted of a single machined piece for each of the three aileron deflections: -10°, 0°, and 10°. Details of the ailerons are presented in figure 1(c). The trailing edge down deflection was assigned the positive value. When installed, the machined piece for the aileron was sealed to the wing along the upstream edge. Ailerons were mounted only on the port wing panel.

The wing contains 258 static-pressure orifices distributed in 7 chordwise rows. (See figure 1(a)). To simplify model fabrication and maximize wing strength, upper-surface orifices are located in the port wing panel and lower-surface orifices are located in the starboard wing panel. The nominal orifice diameter was 0.015 inches.

Instrumentation

Aerodynamic force and moment data were obtained with a six-component, strain-gage balance. Different balances were used for the two tests: the NTF101B balance was used for the outboard spoiler test and the NTF113B balance was used for the outboard aileron test.

An onboard, heated, single-axis accelerometer package was used to measure the model angle of attack. The accelerometer package has a quoted accuracy of ±0.01° under smooth wind-tunnel operating conditions (ref. 4). For the test conditions presented in this report, the model dynamic acceleration was small and was not expected to have a significant impact on the accuracy of the angle of attack measurement.

Wing-pressure measurements were made with six 48-port, electronically scanned pressure (ESP) modules contained in an internal, nose-mounted, heated enclosure. The upper surface (port wing) pressures were measured using modules having a full-scale pressure range of ±45 psid; the lower surface (starboard wing) pressures were measured using modules having a range of ±30 psid. The quoted accuracy of the modules was ±0.20 percent of full scale pressure. The modules were calibrated immediately before each series of runs. Body cavity pressures were measured at two locations inside the fuselage cavity using an ESP module with a full-scale pressure range of ±2.5 psid.

The wind tunnel total and static pressures were measured using two banks of quartz bourdon tube transducers referenced to a vacuum. A controller selects the smallest transducer from each bank capable of measuring the total and the static pressures. The manufacturer's quoted accuracy for these pressure transducers is ±0.012 percent of reading plus ±0.006 percent of full scale. Since data were obtained at three levels of dynamic pressure (to be discussed later), different transducers in each bank were used depending on the test conditions. For the low level dynamic pressure data, 30 psi transducers were used for both the total and static pressure measurements. For the intermediate level dynamic pressure data, 50 psi transducers were used for both the total and static pressure measurements. For the high level dynamic pressure data, a 100 psi transducer was used for the total pressure measurement and a 50 psi transducer was used for the static pressure measurement. The tunnel total temperature was measured with a platinum resistance thermometer with an accuracy of ±0.2°F.

The accuracy of the measurement instruments was used to estimate the error bands for the model force and moment coefficients for the loads encountered near the angle of attack for the design lift coefficient using the technique described in reference 5. Error bands for the force and moment coefficients based on the quoted instrumentation accuracies for the two tunnel tests are presented in table 2. As expected, the uncertainty in each of the force and moment coefficients decreases with increasing dynamic pressure. Changes in results smaller than the measurement uncertainty should not be considered significant.

Procedures

Data Reduction and Corrections

Information on NTF instrumentation devices, tunnel process and data-acquisition systems, and data-reduction algorithms are provided in reference 6. Balance output is sensitive to the balance temperature as well as the balance longitudinal temperature gradient. Balance readings were compensated for changes in balance temperature between the wind-on and wind-off conditions. Also, temperature gradients within the balance were minimized by allowing the balance to approach thermal equilibrium with the tunnel flow before recording any data. Balance-temperature gradients of less than 10°F were maintained throughout these tests. Wind-off data were acquired prior to and following each set of runs to monitor balance electrical zero shifts over the course of a set of runs. The ending wind-off point was used for all data reduction because the thermal state of the balance (for both temperature and temperature gradient) at the end of a set of runs was generally more representative of the wind-on conditions.

The model angle of attack was corrected for upflow in the test section, with the upflow angle determined from data acquired with the model in both upright and inverted orientations at a given set of tunnel conditions. In each test, an upright and inverted run was obtained for each Reynolds number at the design Mach number, 0.82, and the resulting upflow correction applied across the Mach number range. Upflow angles ranged from about 0.13° to about 0.18°. The data used in this report were not corrected for test-section wall interference or for sting interference.

Tests and Procedures

The test program was designed to investigate the effects of Reynolds number at transonic speeds on the performance of different lateral control devices. The Mach number range covered speeds from below the design Mach number (M_∞=0.70) to above the maxi-

mum operating Mach number (M_∞=0.94) of a typical subsonic commercial transport. The lowest Reynolds number was representative of the Reynolds numbers obtained on similarly sized models in conventional transonic wind tunnels ($R_{\bar{c}} = 3\times10^6$). The highest Reynolds number was representative of a moderate sized commercial transport at cruise ($R_{\bar{c}} = 30\times10^6$). Two additional Reynolds numbers ($R_{\bar{c}} = 13\times10^6$ and $R_{\bar{c}} = 22\times10^6$) were included to assess Reynolds number effects. At each test condition, the angle of attack was varied from about -2° (approximately the angle of zero lift) to about 6° (or the onset of model pitch angle dynamics).

The wind tunnel model wing will deform under load. Testing at different dynamic pressures will yield different model loads and, consequently, different model deformations. The effects of model deformation should be removed from the experimental results. Static aeroelastic deformation of the wing depends on the applied load and the material stiffness. An indicator of static aeroelastic deformation is the nondimensional ratio of dynamic pressure (q_∞), to the modulus of elasticity (E) for the metal that comprises the wing. The parameter q_∞/E is appropriate for characterizing aeroelastic condition because the material stiffness E increases as the temperature decreases. To eliminate the effect of static aeroelastic deformation, the model should be tested at constant q_∞/E.

Although the operating characteristics of the NTF allow independent variation of Mach number, Reynolds number, and dynamic pressure, constraints from the NTF operating envelope prevent testing at a constant dynamic pressure across the full range of desired Mach numbers and Reynolds numbers. The NTF operating envelope for the Pathfinder-I Lateral Controls Model at a Mach number of 0.82, shown in figure 2, demonstrates the problem. At transonic conditions, the minimum temperature is typically about -250° and the maximum temperature is about 130°. The need to maintain a positive pressure within the tunnel pressure shell relative to atmospheric pressure determines the minimum dynamic pressure. One option is to test at a high dynamic pressure ($q_\infty/E = 0.61\times10^{-6}$) over a reduced Reynolds number range from about 7×10^6 to 30×10^6. Extensive testing at such high levels of dynamic pressure is not preferred because of the high liquid nitrogen consumption. The desired test matrix could not be completed at this high dynamic pressure because the required liquid nitrogen exceeded the amount available for the test. An alternate approach that limits the testing required at the high dynamic pressure was selected. This approach provides Reynolds number effects at three levels of dynamic pressure and static aeroelastic (i.e. dynamic pressure) effects at two intermediate Reynolds numbers as noted by the solid circles in figure 2. The results at Reynolds numbers 3×10^6 and 13×10^6 are obtained at the baseline $q_\infty/E = 0.28\times10^{-6}$ (low range), the results at a Reynolds number of 22×10^6 are obtained at $q_\infty/E = 0.45\times10^{-6}$ (intermediate range), and the results at a Reynolds number of 30×10^6 are obtained at $q_\infty/E = 0.61\times10^{-6}$ (high range). The results for a Reynolds number of 22×10^6 are corrected for the static aeroelastic increment between $q_\infty/E = 0.45\times10^{-6}$ and $q_\infty/E = 0.28\times10^{-6}$. Similarly, the results for a Reynolds number of 30×10^6 are corrected for two static aeroelastic increments: the first between $q_\infty/E = 0.61\times10^{-6}$ and $q_\infty/E = 0.45\times10^{-6}$ and the second between $q_\infty/E = 0.45\times10^{-6}$ and $q_\infty/E = 0.28\times10^{-6}$.

Each time the model is assembled, small differences in the clean (no deflected control surface) wing are possible, leading to small differences in the baseline rolling moment coefficients. Also, small manufacturing differences created small asymmetries in the model. To minimize these effects, the effect of control surface deflection was determined from the difference between the results with the control surface deflected and the results with the control surface set to 0° (clean wing). Separate clean wing data were obtained for each test.

Clean wing data were not obtained during the outboard spoiler test at the intermediate dynamic pressure level at a Reynolds number of 13×10^6 and the high dynamic pressure at a Reynolds number of 22×10^6 for Mach numbers from 0.70 to 0.88. Estimated clean wing data were needed to determine the increments in the force and moment coefficients due to spoiler deflection. Examination of the increments in the force and moment coefficients from three other wind tunnel tests of the Lateral Controls Wing due to increasing the dynamic pressure from the low to the intermediate levels and from the intermediate to high levels showed similar static aeroelastic effects for each test. Since the static aeroelastic increments are relatively independent of the test, the missing clean wing data were estimated by adding the average static aeroelastic increment from the other three Lateral Controls Wing tests to the available clean wing data from the outboard spoiler test.

All polars were obtained in a "pitch-pause" mode in which the model is pitched to the next angle of attack in the series, transients in the flow and instrumentation are allowed to damp out, and the data are then recorded before repeating the cycle.

Wing pressure data acquisition required ESP hardware (tubing for the reference pressure, calibration

pressure, and control pressure and electrical wires for data acquisition and control) to bridge the balance. Previous test experiences (e.g. ref. 7) indicated that the presence of the ESP instrumentation had a small effect on the lift and pitching moment measurements.

The results at the two lower Reynolds numbers, 3×10^6 and 13×10^6, were obtained with the boundary layer transition location artificially fixed on the nose of the model and on the wing upper and lower surfaces. Epoxy disks were selected for the trip strips because they provide a repeatable configuration unlike carborundum grit (ref. 8). The disks, 0.0035 inches high and 0.045 inches in diameter, were installed with the disk centers 0.100 inches apart. Disk height was determined using the method described in reference 9. The ring of disks on the fuselage nose was located 1.00 inch downstream of the nose (sta = -9.5 in.). The rows of disks on each surface of the wing were laid out in two straight lines, from the wing root to the leading edge break, and from the leading edge break to the tip. The trip location varies from about 0.05c at the root to about 0.10c at the tip. Natural boundary layer transition (strips of trip disks removed) was used for tests at the two higher Reynolds numbers, 22×10^6 and 30×10^6, since transition is estimated to occur within the first 5 percent of the local chord.

Repeatability

The Lateral Controls Wing has been tested three times with the wing-fuselage fillets. Repeat runs were obtained at a Mach number of 0.82 and a Reynolds number of 3×10^6 for the clean wing during each test. These runs were analyzed to assess the data repeatability using the regression statistical analysis of reference 10. The statistical analysis was applied over an angle of attack range from -1° to 3°. The estimated mean value was calculated from a fourth-order polynomial regression equation fitted to the results. From the measured data and the estimated mean value, the residual error, the 95-percent confidence interval, and the 95-percent prediction interval were determined. The 95-percent confidence interval is the bounds about the estimated mean value that encompass the true mean with a 95-percent probability. The 95-percent prediction interval is the bounds about the estimated mean value that will contain a single future measurement with a 95-percent probability. The confidence interval is related to the location of the true mean and the prediction interval is a measure of the data scatter. As defined in reference 10, confidence and prediction intervals are inversely proportional to the number of measurements in the data set and the local density of the measurements. Thus, at the ends of the intervals, the local density of the points decreases and the confidence and prediction intervals widen. The results from the statistical analysis are presented in figure 3. In general, the repeatability is good, with the confidence interval similar in magnitude to the measurement uncertainty.

Results and Discussion

Outboard spoilers

The effect of outboard spoiler deflection for the force and moment coefficients was determined from the increment (difference) in the coefficient with the spoiler deflected and with the clean wing. The increment is denoted by the Δ symbol preceding the coefficient. A sample of the effect of Reynolds number on the increments in the force and moment coefficients is presented in figure 4 for a spoiler deflection of 20° at a Mach number of 0.82. For the lower angles of attack, the increment in rolling moment coefficient due to spoiler deflection is relatively constant. The level generally becomes more negative as the Reynolds number increases from 3×10^6 to 22×10^6. A smaller change is found between Reynolds numbers of 22×10^6 and 30×10^6. It should be noted that these changes in rolling moment coefficient are larger than the test-to-test repeatability ($\approx$0.0002) and the uncertainty in the rolling moment coefficient ($\approx$0.0001 to $\approx$0.0003). As the angle of attack increases above about 2.5°, the increment in rolling moment coefficient becomes less negative. Model pitch dynamics frequently occurred in this part of the test envelope, limiting the extent of the angle of attack range. The yawing moment, pitching moment, and lift coefficient increments show the expected trends. In regions where the rolling moment coefficient is relatively constant, the yawing moment coefficient and the lift coefficient increments are negative and the pitching moment coefficient increment is positive. In regions where the rolling moment coefficient is becoming less negative, the yawing moment and lift coefficient increments are also becoming less negative and the pitching moment coefficient is becoming less positive.

The basic results were curvefit and fitted values at an angle of attack of 0.0° and were cross-plotted to determine the variation of the increment in rolling moment coefficient with Reynolds number for two spoiler deflections and the results are presented in figure 5. In most cases, the increment in rolling moment coefficient due to spoiler deflection becomes more negative as the Reynolds number increases from 3×10^6 to 22×10^6. Typically, there is only a small change in the rolling moment coefficient between Reynolds

numbers of 22×10^6 and 30×10^6. The influence of Reynolds number on the increment in rolling moment coefficient is generally larger for the 20° spoiler deflection.

The basic results were cross-plotted at the same angle of attack to determine the variation of the increment in rolling moment coefficient with spoiler deflection and the results are presented in figure 6. In general, spoiler roll control power, as determined from the slopes of the curves, decreases at the higher Mach numbers. Increasing the Reynolds number generally increased the roll control power.

Reynolds number will have an influence on the wing pressure distributions. Direct comparisons of the pressure distributions on the wing for the different spoiler deflections are not possible because of the differences in the angle of attack for the data at a given Reynolds number, dynamic pressure, and Mach number. At each combination of Reynolds number, dynamic pressure, and Mach number, the pressure coefficient from each pressure orifice was curvefit as a function of angle of attack and fitted values selected at angles of attack of 0° and 4°. Results at Reynolds numbers of 22×10^6 and 30×10^6 were corrected for static aeroelastic effects in a manner similar to that used for the force and moment data.

The effect of Reynolds number on the trailing edge pressure distributions with and without the spoilers deflected is presented in figure 7. Since there was an incomplete set of clean wing data, the undeflected results were taken from the starboard wing panel. For the clean wing, the trailing edge pressure coefficient becomes more positive (less negative) as the Reynolds number increases. Separated flow regions tended to become smaller as the Reynolds number increases. For the spoiler deflected, there is a significant separated flow region downstream of the spoiler, as shown by the negative pressure coefficients at η=-0.44 to η=-0.69. (The spoiler hinge line extended from η=-0.430 to η=-0.669.) At the higher angle of attack, a separated flow region developed on the clean wing near the mid-span portion of the wing. The loss of lift on the clean wing panel from the separated flow region increases so as to reduce the effectiveness of the spoiler on the opposite wing panel.

Outboard ailerons

The effect of Reynolds number on the increments in the force and moment coefficients is presented in figure 8 for an aileron deflection of -10°. For the angles of attack used in this investigation, the increment in rolling moment coefficient due to aileron deflection was relatively constant for Mach a number of 0.82. The magnitude of the increment in the rolling moment coefficient was smallest at a Reynolds number of 3×10^6 and generally increased as the Reynolds number increased. The increment due to aileron deflection in lift coefficient was generally negative and the increment in pitching moment coefficient was positive.

The basic results were curve fit and cross-plotted at an angle of attack of 0° to determine the increment in rolling moment coefficient with Reynolds number for both aileron deflection angles and the results are presented in figure 9. The effect of Reynolds number on the increment in rolling moment coefficient is generally small with a general trend of increasing magnitude with increasing Reynolds number.

The basic results were also cross-plotted to determine the increment in rolling moment coefficient with aileron deflection angle for constant Reynolds number and the results are presented in figure 10. In general, the aileron control power increases with Reynolds number and is larger for the negative aileron deflection.

Pressure data were not obtained for the two lower Reynolds numbers in the outboard aileron test so the effect of Reynolds number on the trailing edge pressure coefficient distribution and the chordwise pressure coefficient distribution could not be determined.

Additional results from the outboard aileron and outboard spoiler wind tunnel tests are available in reference11.

Concluding Remarks

Data from two tests of a wing-body configuration in the NTF have been analyzed to study the effect of Reynolds number on the performance of lateral control devices. The results indicated that:

1. In most cases, the increment in rolling moment due to spoiler deflection becomes more negative as the Reynolds number increases from 3×10^6 to 22×10^6. Typically, there is only a small change in the rolling moment coefficient between Reynolds numbers of 22×10^6 and 30×10^6. The influence of Reynolds number on the increment in rolling moment coefficient is generally larger for the 20° spoiler deflection.

2. For the clean wing configuration, the trailing edge pressure became more positive (less negative) as the Reynolds number increases. Separated flow regions tended to become smaller as the Reynolds number increases.

3. For the aileron deflected configuration, the effect of Reynolds number on the increment in rolling moment coefficient is generally small with a general trend of increasing magnitude with increasing Reynolds number

References

1. Jacobs, Peter F. and Gloss, Blair B.: Longitudinal Aerodynamic Characteristics of a Subsonic, Energy-Efficient Transport Configuration in the National Transonic Facility. NASA TP-2922,. August, 1989.

2. Fuller, D. E.; Gloss, B. B.; and Nystrom, D.: *Guide to Users of the National Transonic Facility.* NASA TM-83124, 1981.

3. Igoe, William B.: *Analysis of Fluctuating Static Pressure Measurements in the National Transonic Facility.* NASA TP-3475, March 1996. (Also available as *Analysis of Fluctuating Static Pressure Measurements of a Large High Reynolds Number Transonic Cryogenic Wind Tunnel.* Ph.D Dissertation, George Washington University, May 1993.)

4. Finley, Tom D.; and Tcheng, Ping: Model Attitude Measurements at NASA Langley Research Center. AIAA-92-0763, Jan. 1992.

5. Coleman, Hugh W; and Steele, W. Glenn: Experimentation and Uncertainty Analysis for Engineers. John Wiley and Sons, 1989.

6. Foster, Jean M.; and Adcock, Jerry B.: *User's Guide for the National Transonic Facility Research Data System.* NASA TM-110242, April 1996.

7. Al-Saadi, Jassim A.: *Effect of Reynolds Number, Boundary-Layer Transition, and Aeroelasticity on Longitudinal Aerodynamic Characteristics of a Subsonic Transport Wing.* NASA TP-3655, 1997.

8. Chan, Y. Y.: Comparison of Boundary Layer Trips of Disks and Grit Types on Airfoil Performance at Transonic Speeds. NAS-AN-56 (NRC-29908), National Aeronautical Establishment (Ottawa, Ontario), Dec. 1988.

9. Braslow, Albert L.; and Knox, Eugene C.: *Simplified Method for Determination of Critical Height of Distributed Roughness Particles for Boundary Layer Transition at Mach Numbers from 0 to 5.* NACA TN 4363. 1958.

10. Wahls, R.A.; Adcock, J. B.; Witkowski, D. P.; and Wright, F. L.: *A Longitudinal Aerodynamic Data Repeatability Study for a Commercial Transport Model Test in the National Transonic Facility.* NASA TP-3522. August 1995.

11. Mineck, Raymond E.: *Reynolds Number Effects on the Performance of Lateral Control Devices.* NASA TM-2000-210541. October 2000.

Table 1: Model Characteristic Dimensions.

Body:	
maximum diameter	5.75 in.
length	60.5 in.
Wing (based on trapezoidal planform):	
aspect ratio	9.8
taper ratio	0.4
sweep, quarter chord	30.0°
dihedral	5.0°
mean geometric chord	5.742 in.
span	52.97 in.
reference area	1.9884 ft^2

Table 2: Uncertainty in Model Force and Moment Coefficients.

	Outboard Spoiler Data, $q_\infty/E\approx$		
Component	$.28\times10^{-6}$	$.45\times10^{-6}$	$.62\times10^{-6}$
C_L	.0031	.0019	.0014
C_m	.0013	.0008	.0006
C_l	.00030	.00018	.00013
C_n	.00018	.00011	.00008
	Outboard Aileron Data, $q_\infty/E\approx$		
Component	$.28\times10^{-6}$	$.45\times10^{-6}$	$.62\times10^{-6}$
C_L	.0025	.0016	.0011
C_m	.0010	.0006	.0004
C_l	.00019	.00012	.00008
C_n	.00008	.00005	.00004

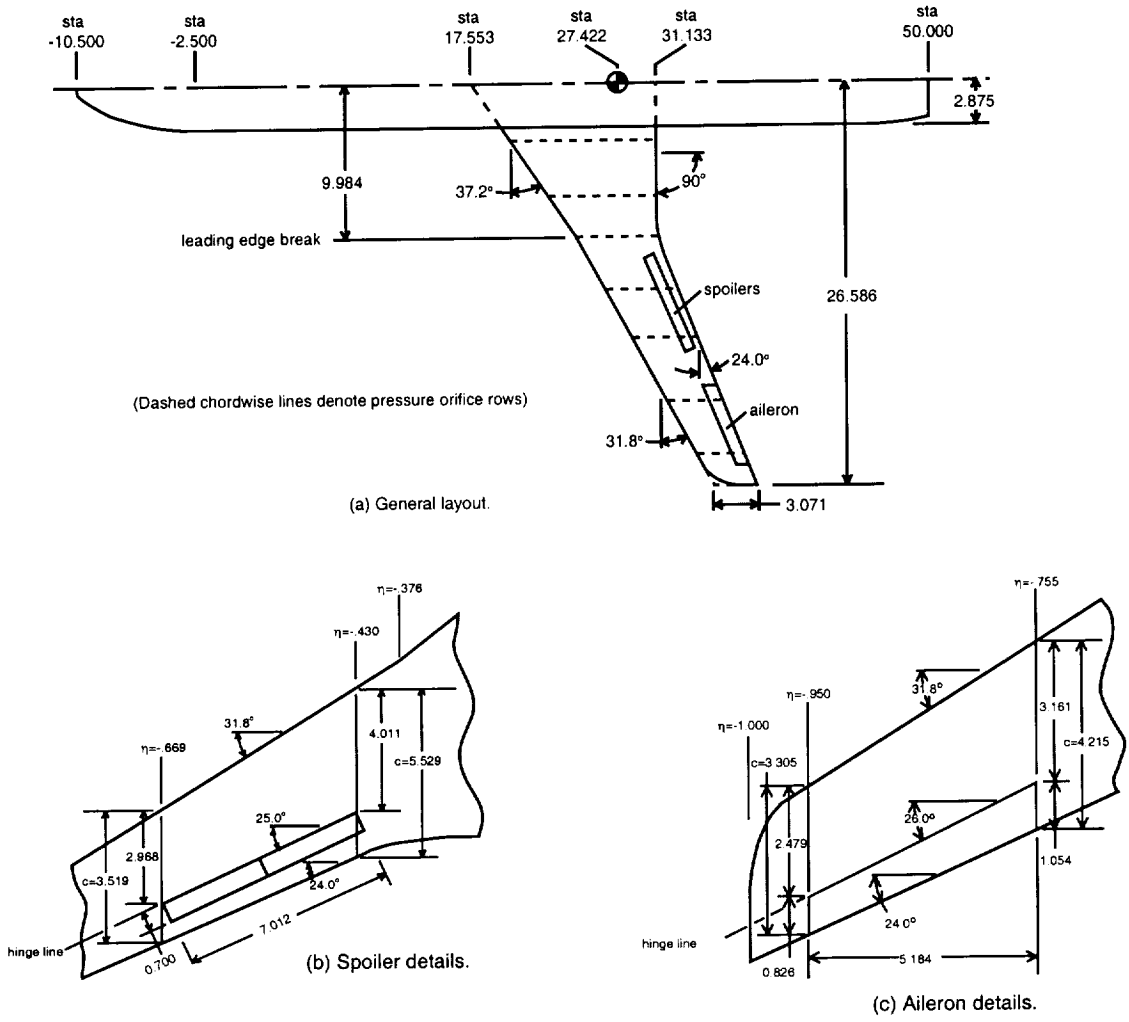

Fig. 1. Details of the model. (All linear dimensions in inches).

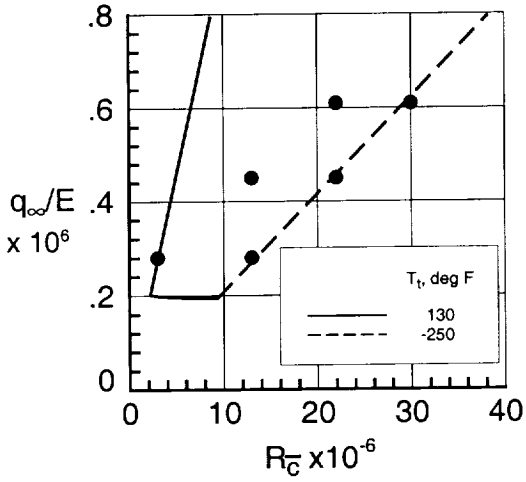

Fig. 2. Operating envelope for model at $M_\infty = 0.82$.

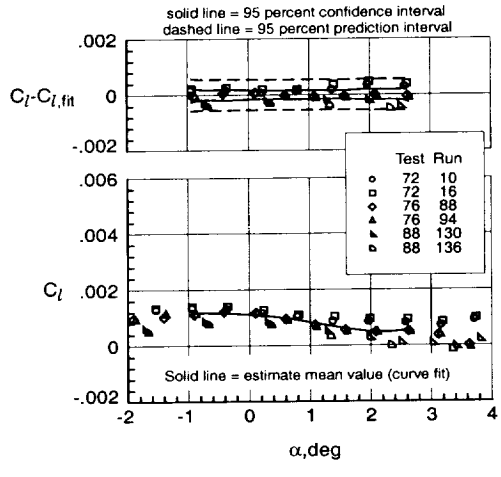

Fig. 3. Test to test repeatability of C_l.

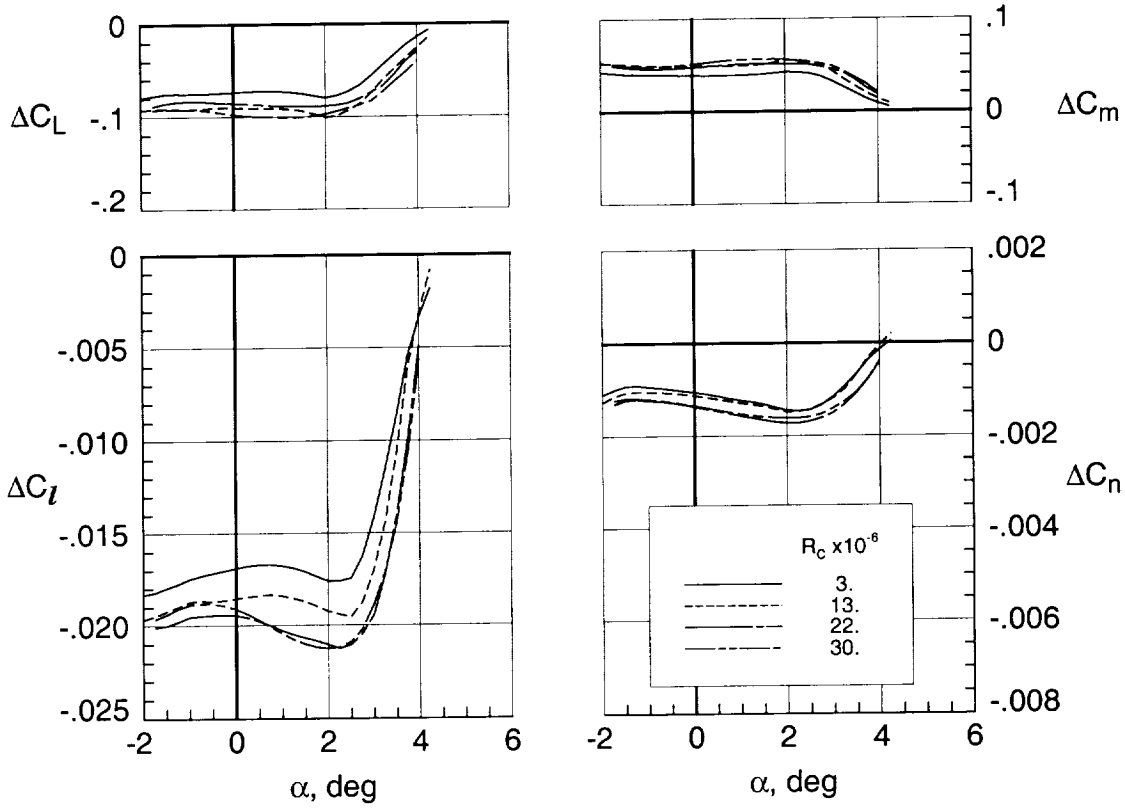

Fig. 4. Variation of the force and moment coefficients with angle of attack. δ_s=20°. M_∞=0.82.

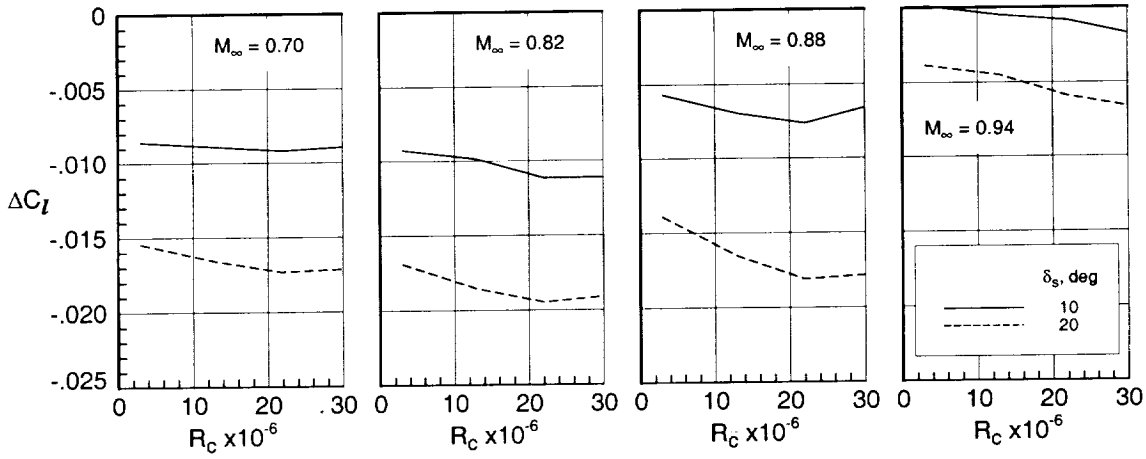

Fig. 5. Variation of rolling moment coefficient with Reynolds number with deflected spoilers. α = 0°.

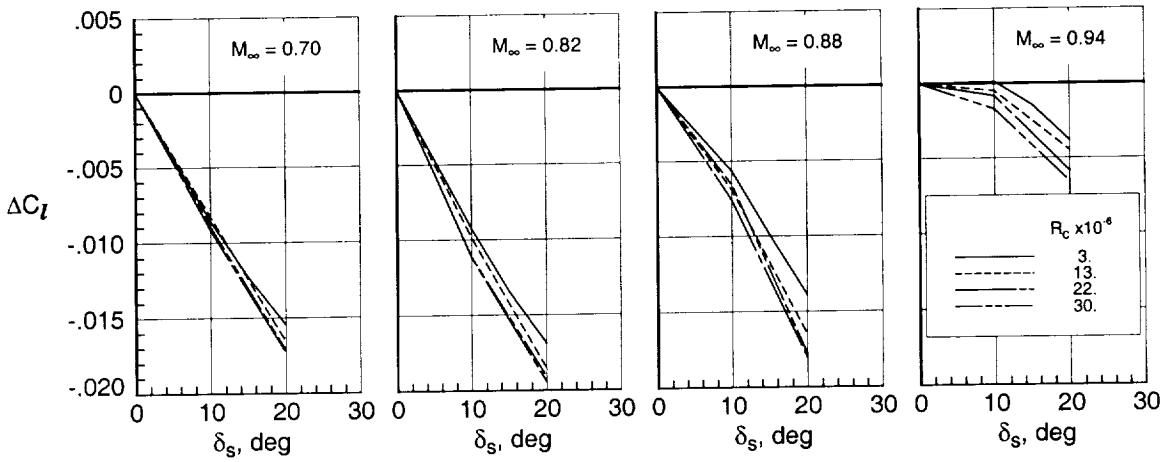

Fig. 6. Variation of rolling moment coefficient with spoiler deflection. $\alpha = 0°$.

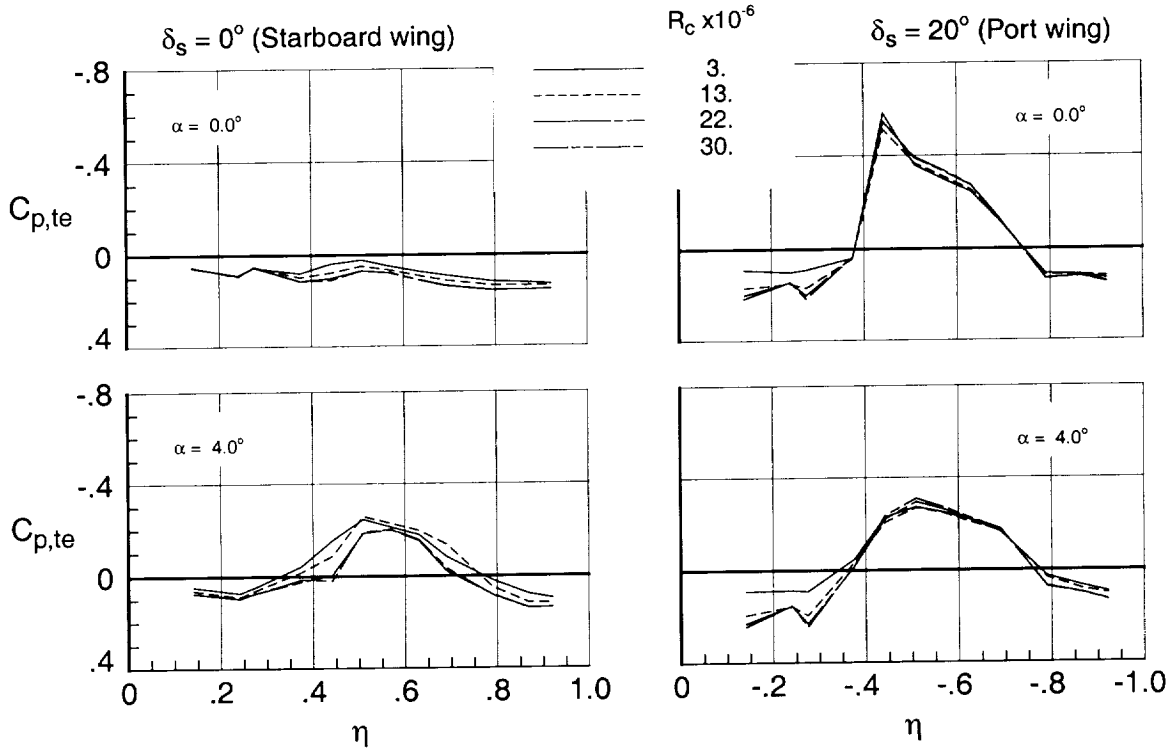

Fig. 7. Variation of the trailing edge pressure coefficient distribution with Reynolds number. M_∞=0.82.

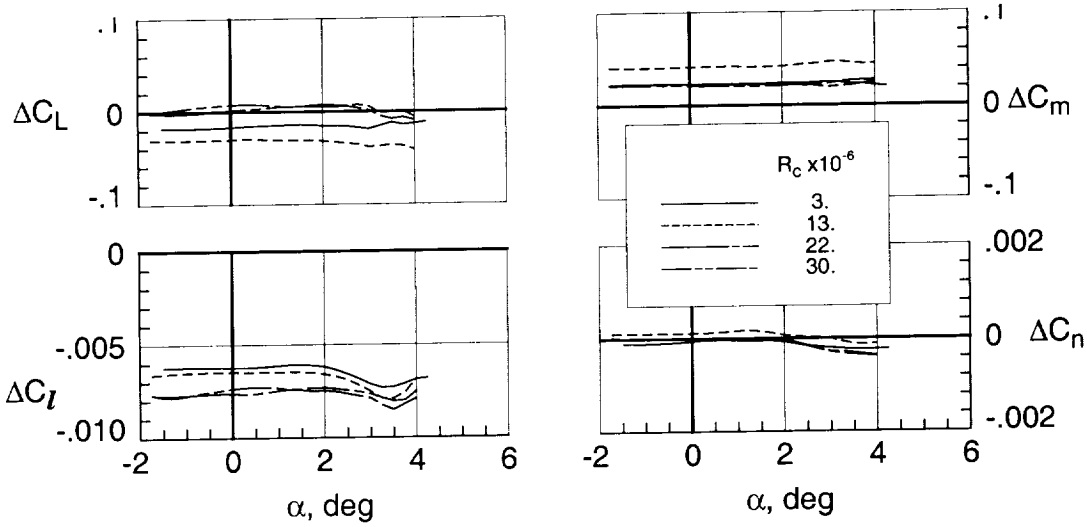

Fig. 8. Variation of the rolling moment coefficient with angle of attack with deflected ailerons. δ_a=-10°. M_∞=0.82.

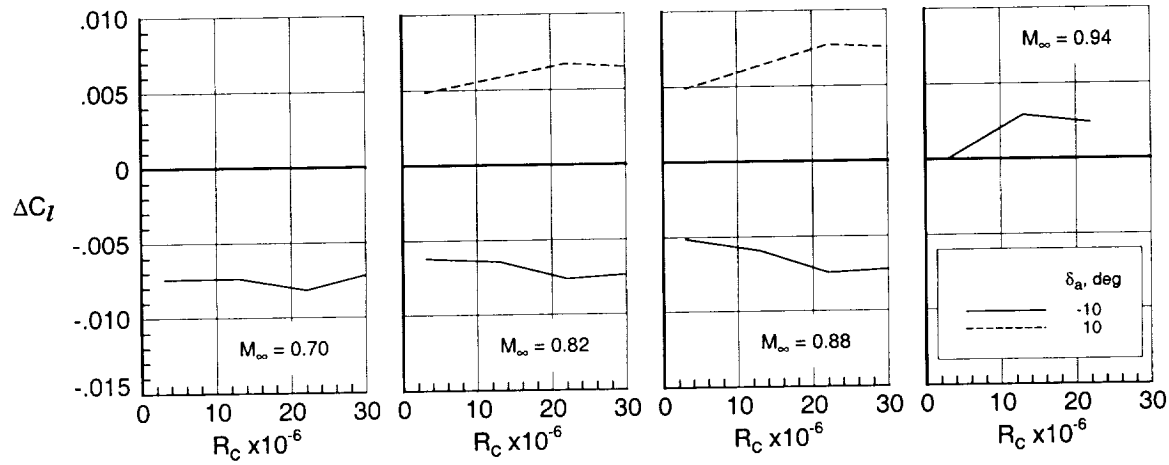

Fig. 9. Variation of rolling moment coefficient with Reynolds number with deflected ailerons. $\alpha = 0°$.

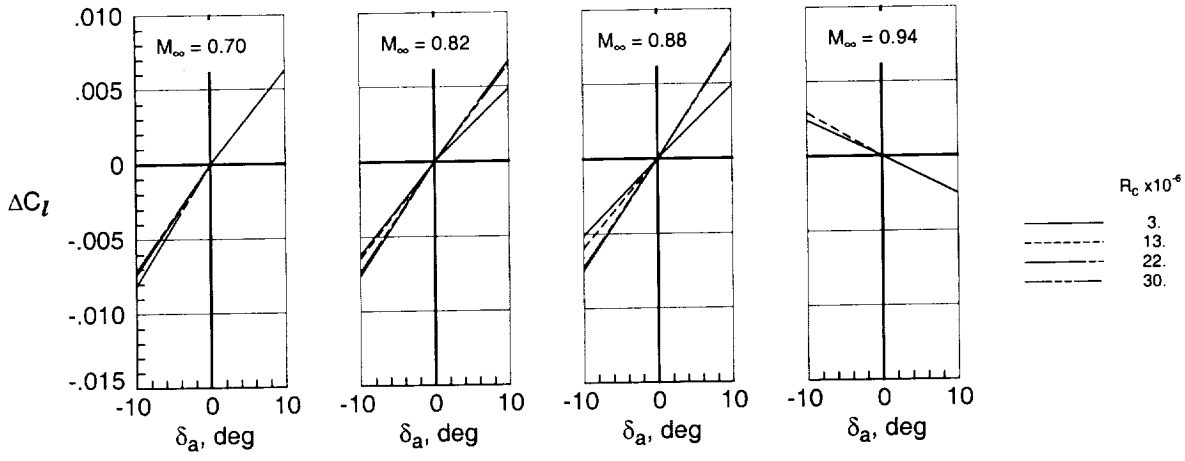

Fig. 10. Variation of rolling moment coefficient with aileron deflection. $\alpha = 0°$.